

K^-p correlation function from high-energy nuclear collisions and chiral SU(3) dynamics

Yuki Kamiya,^{1,*} Tetsuo Hyodo,^{2,3} Kenji Morita,^{4,5} Akira Ohnishi,² and Wolfram Weise^{6,7}

¹CAS Key Laboratory of Theoretical Physics, Institute of Theoretical Physics, Chinese Academy of Sciences, Beijing 100190, China

²Yukawa Institute for Theoretical Physics, Kyoto University, Kyoto 606-8502, Japan

³Department of Physics, Tokyo Metropolitan University, Hachioji 192-0397, Japan

⁴RIKEN Nishina Center, Wako 351-0198, Japan

⁵National Institutes for Quantum and Radiological Science and Technology,

Rokkasho Fusion Institute, Rokkasho, Aomori, 039-3212, Japan

⁶Physics Department, Technical University of Munich, D-85748 Garching, Germany

⁷ExtreMe Matter Institute (EMMI) at GSI, D-64291 Darmstadt, Germany

(Dated: November 5, 2019)

The two-particle momentum correlation function of a K^-p pair from high-energy nuclear collisions is evaluated in the $\bar{K}N$ - $\pi\Sigma$ - $\pi\Lambda$ coupled-channels framework. The effects of all coupled channels together with the Coulomb potential and the threshold energy difference between K^-p and \bar{K}^0n are treated completely for the first time. Realistic potentials based on the chiral SU(3) dynamics are used which fit the available scattering data. The recently measured correlation function is found to be well reproduced by allowing variations of the source size and the relative weight of the source function of $\pi\Sigma$ with respect to that of $\bar{K}N$. The predicted K^-p correlation function from larger systems, which is less affected by the $\pi\Sigma$ source function, indicates that the investigation of its source size dependence is useful in providing further constraints in the study of the $\bar{K}N$ interaction.

PACS numbers: 25.75.Gz, 21.30.Fe, 13.75.Ev

Introduction: Low-energy properties of the strong interaction are governed by the symmetry breaking pattern of quantum chromodynamics (QCD). In this context the antikaon ($\bar{K} \sim s\bar{u}/s\bar{d}$) can be regarded as a Nambu-Goldstone boson associated with the spontaneous breaking of three-flavor chiral symmetry. However, its mass is more than three times heavier than that of pions, given the strange quark mass of about 100 MeV. Thus, studies involving the antikaon reflect the interplay between spontaneous and explicit breakings of chiral symmetry in low-energy QCD.

The antikaon-nucleon ($\bar{K}N$) interaction at low energy is strongly attractive. It is the main ingredient to generate the $\Lambda(1405)$ resonance as a $\bar{K}N$ quasi-bound state [1]. This observation inspired an intense discussion of possible \bar{K} -nuclear quasi-bound systems [2]. A possible candidate is recently reported by the J-PARC E15 Collaboration [3].

Contrary to its importance in hadron physics and also in nuclear many-body problems with strangeness, empirical information on the low-energy $\bar{K}N$ interaction is quite limited. The K^-p scattering amplitude close to threshold is accurately constrained by the measurement of the atomic energy shift and width of K^- hydrogen [4]. There exist several K^-p cross section data at relatively high momenta, $p_{\text{Lab}}(K^-) > 100$ MeV/c [5]. However, the uncertainties of the cross sections from the bubble chamber measurements are large, and almost no data exist in the low-momentum region, $p_{\text{Lab}}(K^-) \leq 100$ MeV/c.

One of the promising observables that provides stronger constraints on the $\bar{K}N$ interaction is the two-particle K^-p momentum correlation function. It is defined as the two-particle production probability normalized by the product of single-particle production probabilities [6, 7]. Theoretically, the correlation function reflects the two-body interac-

tions through the wave function with a suitable boundary condition. On the experimental side, correlation functions have been measured for $p\Lambda$ [8, 9], $\Lambda\Lambda$ [9, 10], $p\Xi^-$ [11], $p\Omega$ [12], pK^- [13], and $p\Sigma^0$ [14] pairs. These data have been used to constrain the pairwise interactions [7, 15–19]. Recently the K^-p correlation function has been extracted from high-multiplicity events of pp collisions [13]. The precision and the resolution of these data are so excellent that the \bar{K}^0n threshold cusp is visible. Several data points exist also in the energy region below the \bar{K}^0n threshold. In addition the data show a peak in the energy region of the $\Lambda(1520)$ resonance which couples to the $\bar{K}N$ d -wave.

For the detailed analysis of the K^-p strong interaction in comparison with the high-precision data it is mandatory to include the coupled-channels effects, the Coulomb interaction in the K^-p system, and the threshold energy differences among the isospin multiplets in calculating the correlation function. While theoretical studies of the K^-p correlation function have been reported in Refs. [7, 16, 18], there is so far no work which takes account of all of these effects.

In the present article we investigate the K^-p correlation function by developing and using a proper coupled-channels framework. Calculations are performed in the charge basis. Six channels (K^-p , \bar{K}^0n , $\pi^-\Sigma^+$, $\pi^0\Sigma^0$, $\pi^+\Sigma^-$ and $\pi^0\Lambda$) are taken into account, and the coupled-channels version of the correlation function formula [18, 20] is used. Coulomb interactions between charged particles are treated consistently. The threshold energy differences among the various channels are taken into account when solving the coupled-channels Schrödinger equation. In practice we have adopted the realistic $\bar{K}N$ - $\pi\Sigma$ - $\pi\Lambda$ coupled-channels potential [21]. This potential is constructed starting from chiral SU(3) dynamics [22] and systematic fitting to the existing K^-p data. It will be

demonstrated that the K^-p correlation function recently measured by the ALICE collaboration [13] is well explained by our calculations with reasonably tuned source size (R) and the source weight in the $\pi\Sigma$ channels ($\omega_{\pi\Sigma}$). It is found that the effects of coupled channels are important in two ways, the modification of the wave functions in the K^-p channel and the conversion to K^-p from $\pi\Sigma$ generated from the $\pi\Sigma$ source function.

Formalism: In high-energy heavy-ion collisions and high-multiplicity events of pp and pA collisions, the hadron production yields are well described by the statistical model: hadrons are produced almost independently, with source functions that behave smoothly in r -space. Under such conditions the correlations between outgoing particles are considered to be generated by the quantum mechanical scattering in the final state.

Consider two asymptotically observed particles, a and b , with relative momentum $\mathbf{q} = (\mathbf{p}_a - \mathbf{p}_b)/2$ in the pair rest frame. Let this two-particle state be fed by a set of coupled channels, each denoted by j . In the center-of-mass frame of the two measured particles (a, b), their correlation function $C(\mathbf{q})$ is given as [18, 23]:

$$C(\mathbf{q}) = \int d^3r \sum_j \omega_j S_j(\mathbf{r}) |\Psi_j^{(-)}(\mathbf{q}; \mathbf{r})|^2, \quad (1)$$

where the wave function $\Psi_j^{(-)}$ in the j -th channel is written as a function of the relative coordinate \mathbf{r} in that chan-

nel, with outgoing boundary condition for the measured channel. Furthermore, $S_j(\mathbf{r})$ and ω_j are the (normalized) source function and its weight in the j -th channel. The correlation function carries the information, through the wave functions $\Psi_j^{(-)}$, about the interactions in the channels j contributing to the final state under consideration. One can extract this information by properly determining the source function (e.g., by combined fit to data or constraints from other measurements) or by controlling the influence of the source function (e.g., by varying the system size as advocated in Ref. [24].)

We concentrate on the small $q = |\mathbf{q}|$ region and assume that only the s -wave part of the wave function is modified by the strong interaction. The j -th channel component of the wave function with outgoing boundary condition in the K^-p channel (channel 1) is given as

$$\Psi_j^{(-)}(\mathbf{q}; \mathbf{r}) = [\phi^C(\mathbf{q}; \mathbf{r}) - \phi_0^C(qr)]\delta_{1j} + \psi_j^{(-)}(q; r), \quad (2)$$

where $r = |\mathbf{r}|$ and $\phi^C(\mathbf{q}; \mathbf{r})$ is the free Coulomb wave function in the K^-p channel, $\phi_0^C(qr)$ is its s -wave component, and $\psi_j^{(-)}(q; r)$ represents the s -wave function that includes both strong and Coulomb potential effects in the j -th channel. This wave function is subject to the outgoing boundary condition in the K^-p channel as specified below.

The wave function $\psi_j^{(-)}(q; r)$ is computed by solving the coupled-channels Schrödinger equation

$$\begin{pmatrix} -\frac{\nabla^2}{2\mu_1} + V_{11}(r) & V_{12}(r) & \cdots \\ V_{21}(r) & -\frac{\nabla^2}{2\mu_2} + V_{22}(r) + \Delta_2 & \cdots \\ \vdots & \vdots & \ddots \end{pmatrix} \begin{pmatrix} \psi_1(q; r) \\ \psi_2(q; r) \\ \vdots \end{pmatrix} = E \begin{pmatrix} \psi_1(q; r) \\ \psi_2(q; r) \\ \vdots \end{pmatrix}, \quad (3)$$

where the channel indices $j = 1, \dots, 6$ stand for K^-p , \bar{K}^0n , $\pi^-\Sigma^+$, $\pi^0\Sigma^0$, $\pi^+\Sigma^-$ and $\pi^0\Lambda$, in this order; μ_j and Δ_j represent the reduced mass in channel j and the threshold energy difference relative to channel 1, respectively. The diagonal potentials $V_{jj}(r)$ include the Coulomb term, $-\alpha/r$, in channels 1, 3, and 5 in addition to the strong interaction. The off-diagonal potentials are given by the strong interaction only. The momentum in channel j is $q_j = \sqrt{2\mu_j(E - \Delta_j)}$ with $q \equiv q_1$ and $\Delta_1 = 0$. Through this relation, all the momenta q_j can be expressed as functions of q . The Schrödinger equation is then solved with the following boundary condition at $r \rightarrow \infty$:

$$\psi_j^{(-)}(q; r) \rightarrow \frac{1}{2iq_j} \left[\delta_{1j} \frac{u_j^{(+)}(q_j r)}{r} + A_j(q) \frac{u_j^{(-)}(q_j r)}{r} \right] \quad (4)$$

for open channels ($E > \Delta_i$), where $u_j^{(+)}$ and $u_j^{(-)}$ are the

outgoing and incoming waves with a coefficient $A_j(q)$. In contrast to the standard scattering problem with normalized flux of the incoming wave in the incident channel, it is the outgoing wave in the measured channel that is normalized for the calculation of the correlation function. In absence of the Coulomb interaction, the $u_j^{(\pm)}/r$ are the spherical waves, $u_j^{(\pm)}(qr)/r = e^{\pm iqr}/r$, and the coefficient $A_j(q)$ is given by $\sqrt{(\mu_j q_j)/(\mu_1 q_1)} \mathcal{S}_{1j}^\dagger(q_1)$, with the S-matrix \mathcal{S} . Including the Coulomb interaction we have $u_j^{(\pm)}(qr) = \pm e^{\mp i\sigma_j} [iF(qr) \pm G(qr)]$ with $\sigma_j = \arg\Gamma(1 + i\eta_j)$, $\eta_j = -\mu_j\alpha/q_j$, and the regular (irregular) Coulomb functions $F(qr)$ [$G(qr)$]. For closed channels ($E < \Delta_i$), the asymptotic form is given by substituting $q_j = -i\kappa_j = -i\sqrt{2\mu_j(\Delta_j - E)}$ as $\psi_j^{(-)}(r) \rightarrow A_j(q) u_j^{(-)}(-i\kappa_j r)/(2iq_j r) \propto e^{-\kappa_j r}$. This is because the wave function component of the off-shell state can emerge only in the strong interaction region. For spherically symmet-

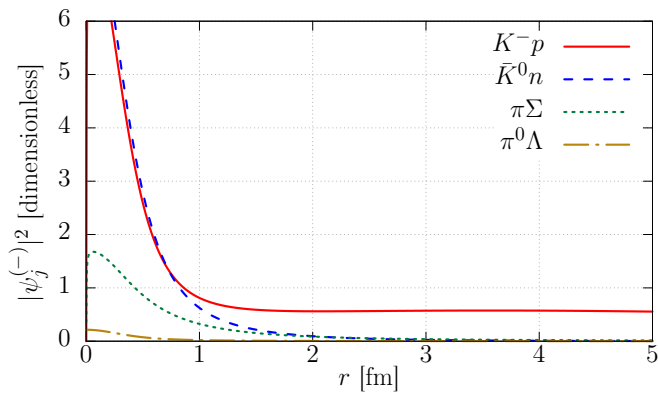


FIG. 1. The modulus square of each component of the coupled-channels wave function with $q = 30$ MeV/c. The solid, dashed, dotted, and dash-dotted lines denote the K^-p , \bar{K}^0n , $\pi\Sigma$, and $\pi^0\Lambda$ component. The $\pi\Sigma$ component is the sum of three components, $\pi^-\Sigma^+$, $\pi^0\Sigma^0$ and $\pi^+\Sigma^-$.

ric source functions, $S_j(\mathbf{r}) = S_j(r)$, the correlation function can be written as

$$C(q) = \int d^3r S_1(r) [|\phi^C(\mathbf{q}; \mathbf{r})|^2 - |\phi_0^C(qr)|^2] + 4\pi \sum_j \int_0^\infty dr r^2 \omega_j S_j(r) |\psi_j^{(-)}(q; r)|^2, \quad (5)$$

where the left-hand side depends only on $q = |\mathbf{q}|$ after the angular integration. The normalization of the source function implies that the weight of the observed channel must be unity: $\omega_1 = 1$ [20]. Note that the first line in Eq. (5) is independent of the strong interaction while the second line represents the strong interaction and coupled-channels effects.

The K^-p correlation function was calculated in Ref. [7] using the effective $\bar{K}N$ potential in Ref. [25] within the model space of K^-p and \bar{K}^0n channels. Although the effects of the coupled $\pi\Sigma$ and $\pi\Lambda$ channels are implicitly included in the renormalized $\bar{K}N$ potential to reproduce the scattering amplitude, the proper boundary condition (4) was not imposed because the wave function does not have explicit $\pi\Sigma$ and $\pi\Lambda$ components. The present calculation reduces to that in Ref. [7] when the channel couplings of $\bar{K}N \leftrightarrow \pi\Sigma, \pi\Lambda$ are switched off. It turns out, however, that there are sizable deviations of the present results from those in Ref. [7]. This indicates the importance of an explicit treatment of coupled channels in the K^-p correlation function.

We now focus on the wave functions in the full $\bar{K}N$ - $\pi\Sigma$ - $\pi\Lambda$ coupled-channels framework. The starting point is chiral SU(3) dynamics at next-to-leading order [22] which successfully describes the set of existing K^-p scattering data together with the SIDDHARTA kaonic hydrogen data [4]. An equivalent local $\bar{K}N$ - $\pi\Sigma$ - $\pi\Lambda$ coupled-channels potential has been constructed to reproduce the corresponding scattering amplitudes [21]. Fig. 1 shows the modulus-squared wave functions $|\psi_j^{(-)}|^2$ with $j = K^-p, \bar{K}^0n, \pi\Sigma$ and $\pi^0\Lambda$, applying the K^-p

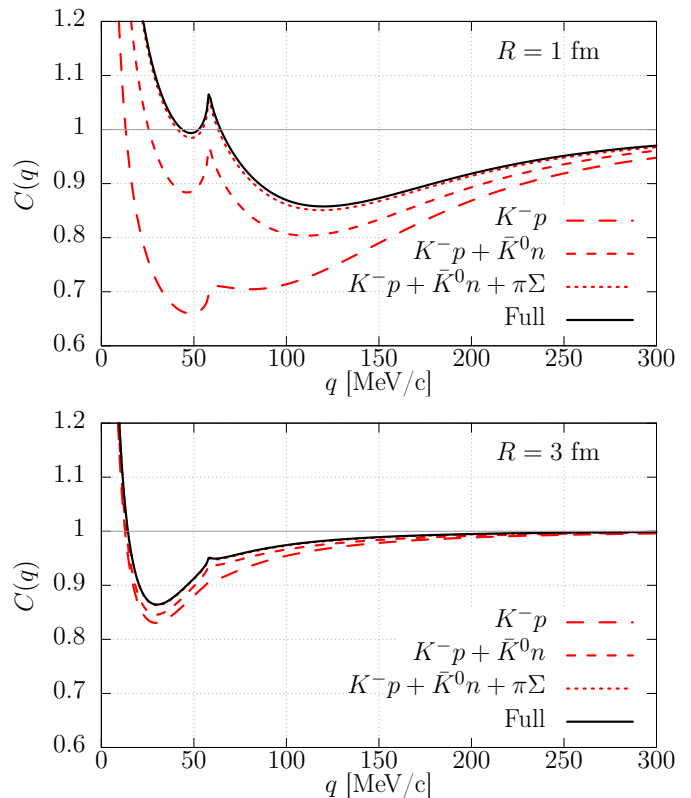


FIG. 2. K^-p correlation function with $R = 1$ fm (upper panel) and $R = 3$ fm (lower panel). The long-dashed line denotes the result with K^-p component only. The dashed, dotted, and solid lines show the results in which the contributions from \bar{K}^0n , \bar{K}^0n and $\pi\Sigma$, and from all coupled-channel components are added, respectively.

outgoing boundary condition at $q = 30$ MeV/c. The squared $\pi\Sigma$ wave function represents the sum of $\pi^-\Sigma^+$, $\pi^0\Sigma^0$ and $\pi^+\Sigma^-$ components. We find that the wave functions in channels other than K^-p have a sizable magnitude at small distances, while they are much smaller than that of K^-p at large distances. From this figure we conclude that contributions from non- K^-p components to the K^-p correlation function are large for small-size sources, while the K^-p component dominates for large sources. Note that the coupled-channels effects contribute to the correlation function through the wave functions $\psi_j^{(-)}$ as well as $\psi_{K^-p}^{(-)}$. This is because $\psi_{K^-p}^{(-)}$ itself is affected by the coupling to the other channels.

Results: The K^-p correlation function and its breakdown into channels is shown in Fig. 2 for source sizes of $R = 1$ fm and 3 fm. We assume a common source function of Gaussian shape for all channels, $S_j(r) = S_R(r) \equiv \exp(-r^2/4R^2)/(4\pi R^2)^{3/2}$ with $\omega_j = 1$. For both source radii R we can see the strong enhancement due to the Coulomb attraction at small momenta and the cusp structure at the \bar{K}^0n threshold at $q \simeq 58$ MeV/c. Among the coupled-channel components, the enhancement by the \bar{K}^0n channel is found to be the largest, and next in importance is $\pi\Sigma$. The in-

clusion of the $\bar{K}^0 n$ component also makes the cusp structure more prominent. The $\pi^0 \Lambda$ channel couples to $K^- p$ only in the $I = 1$ sector; its effect is relatively weak. As expected from the previous discussions, the contributions from the coupled-channel wave function components decrease with increasing source size. This leads to a less pronounced cusp structure for the $R = 3$ fm case.

Now we are prepared to compare the calculated $K^- p$ correlation function with data. We allow for variations of the source functions because the sources and their weights can be channel dependent [18]. Since a given source function in the relative coordinate is obtained from a product of single-particle emission functions, its weight should be proportional to the product of particle yields. For example, $\omega_{\pi^- \Sigma^+} / \omega_{K^- p} = N(\pi^-)N(\Sigma^+) / N(K^-)N(p)$. The production yields $N(h)$ should be regarded as those of *promptly* emitted particles in order for those hadrons to couple with $K^- p$. Thus a particle pair yield ratio such as $N(\pi^-)N(\Sigma^+) / N(K^-)N(p)$ is not a direct observable, and we regard the source weights, ω_j , as parameters. As a reference value, we consider the simplest statistical model estimate, $\omega_{\pi\Sigma}^{(\text{stat})} \simeq \exp[(m_K + m_N - m_\pi - m_\Sigma)/T_c] \simeq 2.1$, where we adopt $T_c = 154$ MeV. By assuming that the source size R is common to all channels and the source function is isospin symmetric, we adopt a common (normalized) source function, $S_j(r) = S_R(r)$. We can fix $\omega_{\pi^0 \Lambda} = 1$ since the effect of the $\pi^0 \Lambda$ channel is small and the correlation function does not depend significantly on $\omega_{\pi^0 \Lambda}$. On the other hand, the effects of $\pi\Sigma$ channels are important because of the strong $\bar{K}N$ - $\pi\Sigma$ coupling, and we vary the parameter $\omega_{\pi\Sigma}$ around the reference value. As for the source size, the ALICE collaboration fixed $R = 1.18$ fm by assuming the same source size as that of $K^+ p$, which was obtained by the femtoscopic correlation fit based on the Jülich $K^+ p$ interaction [18], with Coulomb effects treated by the Gamow factor correction. Although this correction describes the Coulomb effect well for light systems such as π - π , it lacks the necessary accuracy for heavier systems [24]. Thus we also consider the variation of R in the fitting procedure. While the source size can in principle be channel dependent, possible size differences between channels can be compensated by varying the source weights. We therefore use a common source size in $\bar{K}N$, $\pi\Sigma$ and $\pi\Lambda$ channels.

The measured correlation function is assumed to be described in the form [13]

$$C_{\text{fit}}(q) = \mathcal{N} [1 + \lambda \{C(q) - 1\}], \quad (6)$$

where \mathcal{N} is a normalization constant and λ is the pair purity parameter, known also as the chaoticity parameter. The pair purity parameter is experimentally determined through a Monte Carlo simulation, $\lambda_{\text{exp}} = 0.64 \pm 0.06$, so we allow for variations of λ within 1σ . We fit the correlation function data in the momentum range $q < 120$ MeV/ c , where the distortion of the s -wave is considered to give the dominant contribution.

In Fig. 3 the $\chi^2/\text{d.o.f.}$ distribution is plotted in the $(R, \omega_{\pi\Sigma})$ plane. A good fit ($\chi^2/\text{d.o.f.} \lesssim 1$) is achieved in the

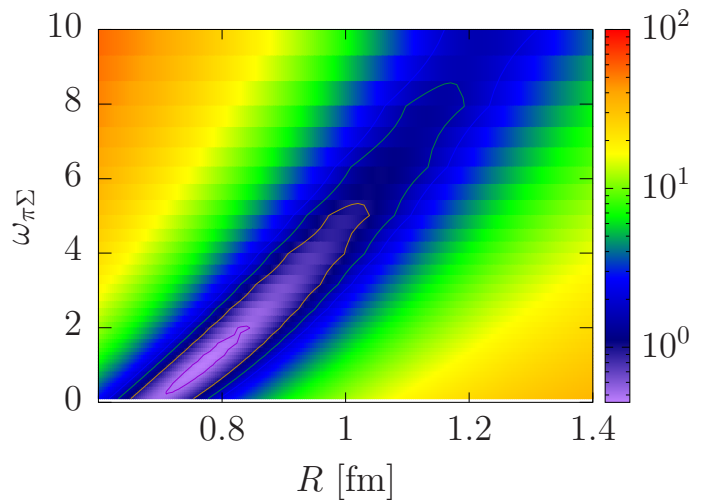


FIG. 3. Reduced χ^2 distribution in the $(R, \omega_{\pi\Sigma})$ plane. From inward out the contour lines correspond to $\chi^2/\text{d.o.f.} = 0.5, 1, 1.5$ and 2 , respectively.

region from $(R, \omega_{\pi\Sigma}) = (0.6 \text{ fm}, 0)$ to $(1.1 \text{ fm}, 5.0)$. These parameters are seen to be in a reasonable range: R is about 1 fm for pp collisions while $\omega_{\pi\Sigma}$ is consistent with the simple statistical model estimate within a factor of $(2 - 3)$. Thus we consider parameter sets in this region with $0.5 \leq \omega_{\pi\Sigma} \leq 5$ as equally acceptable. On the other hand, if we take the $R = 1.18$ fm as adopted by the ALICE collaboration, $\omega_{\pi\Sigma} \gtrsim 8$ gives a good fit, whereas such large $\omega_{\pi\Sigma}$ values appear to be significantly beyond the statistical model estimate.

Fig. 4 shows the fitted $K^- p$ correlation function with $R = 0.9$ fm as an example of a result satisfying $\chi^2/\text{d.o.f.} < 1$. The other parameters are chosen as

$$\omega_{\pi\Sigma} = 2.95, \quad \mathcal{N} = 1.13, \quad \lambda = 0.58, \quad (7)$$

to give the minimum value of $\chi^2/\text{d.o.f.} = 0.58$. The enhancement in the low-momentum range and the characteristic cusp structure are evidently well reproduced. The contribution from the $\pi\Sigma$ source is essential to reproduce the data.

The peak structure seen in Fig. 4 around $q \sim 240$ MeV/ c represents the $\Lambda(1520)$ resonance. The contribution from this resonance can be simulated by a Breit-Wigner function:

$$C_{\text{res}}(q) = \frac{b\Gamma^2}{(q^2/2\mu_{K^- p} + m_p + m_{K^-} - E_R)^2 + \Gamma^2/4}, \quad (8)$$

with parameters b , E_R , and Γ . We can isolate the resonance by subtracting $C_{\text{fit}}(q)$ from the correlation data, using the parameters of Eq. (7) and $R = 0.9$ fm. The remaining structure in the interval $150 \text{ MeV}/c < q < 300 \text{ MeV}/c$ is then fitted by Eq. (8). The resulting values of the resonance parameters are $E_R = 1520.9$ MeV and $\Gamma = 9.7$ MeV, consistent with the mass $M_{\Lambda(1520)} = 1517 \pm 4$ MeV and width $\Gamma_{\Lambda(1520)} = 15_{-8}^{+10}$ MeV of $\Lambda(1520)$ listed in Ref. [26]. As shown in Fig. 4, the sum of $C_{\text{fit}}(q)$ and $C_{\text{res}}(q)$ reproduces the peak at $q \sim 240$ MeV very well.

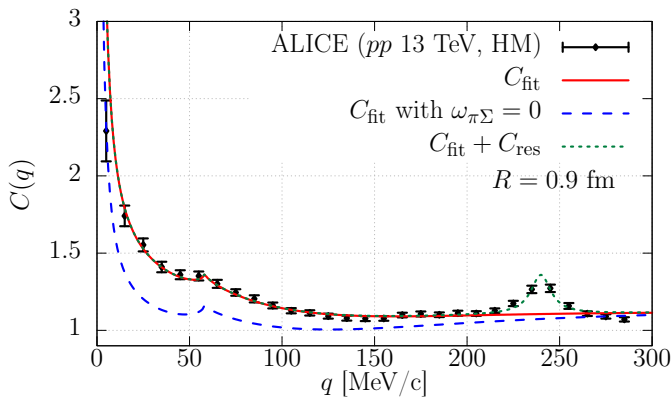


FIG. 4. Correlation function with the best fit values of \mathcal{N} , λ and $\omega_{\pi\Sigma}$ at $R = 0.9$ fm (solid line). To demonstrate the effect of the $\pi\Sigma$ channel, the correlation function with the $\pi\Sigma$ contribution subtracted is also plotted by the dashed line. The fitting result with the $\Lambda(1520)$ contribution is shown by the dotted line. The ALICE data set is taken from Ref. [13].

Finally we give predictions for the K^-p correlation function if extracted from larger systems. In pA and AA collisions the source size is expected to be larger than the one in pp collisions: $R = (1-2)$ fm for high-multiplicity events in pA collisions and $R = (2-5)$ fm in AA collisions. Fig. 5 shows the theoretical correlation function, Eq. (6), at a system size of $R = 1.6$ fm, using the same parameter set as before, Eq. (7), for demonstration. In order to estimate the uncertainty coming from the less well known $\omega_{\pi\Sigma}$, we vary its value between 0.5 and 5.0. One expects that when the source size is increased, the enhancement of the correlation function is limited to the small q region and the \bar{K}^0n cusp becomes less pronounced. The sensitivity to $\omega_{\pi\Sigma}$ is weaker for the larger systems, for which the contribution from the $\pi\Sigma$ source is less important.

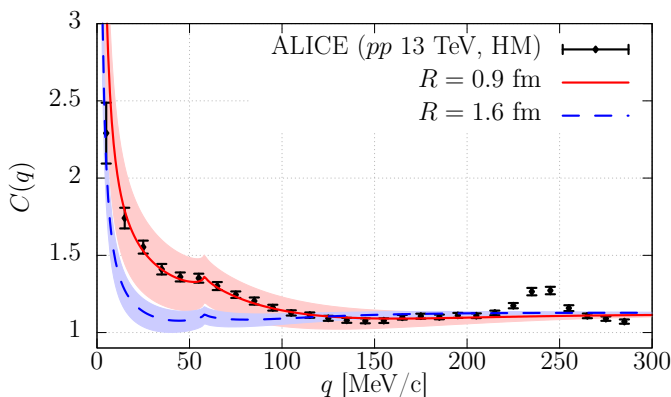


FIG. 5. K^-p correlation for a larger system with $R = 1.6$ fm. The uncertainty with respect to the variation of $\omega_{\pi\Sigma}$ is shown by the shaded area. For comparison we also plot the case of $R = 0.9$ fm.

Summary: The K^-p femtoscopic correlation function has

been analysed using the realistic coupled-channels potential [21]. This potential is constructed based on the amplitudes resulting from next-to-leading order chiral SU(3) dynamics [22]. Based on the coupled-channels correlation function formula [18, 20], we have developed a scheme to calculate the correlation function consistently including all effects of coupled channels, Coulomb potential and threshold differences in the individual channels. The coupled channels play an important role, enhancing the correlation function producing a prominent threshold cusp effect. The K^-p correlation function data obtained by the ALICE collaboration [13] are well reproduced with reasonable source parameters. The allowed value of the source function weight, $\omega_{\pi\Sigma}$, of the $\pi\Sigma$ channel is roughly consistent with a statistical model estimate. The source size ($R = 0.8-1$ fm) is slightly smaller than that determined from the analysis of the K^+p correlation function [13]. This suggests an updated further study of the K^+p correlation function to be performed, including a proper treatment of the full Coulomb effect.

We have also presented a prediction of the K^-p correlation function for a generic larger system. In this case the driving coupled channels become less important as the source size increases. Such correlation functions extracted from collisions of larger systems could provide additional systematics for probing and constraining the K^-p amplitude in low-energy regions not accessible by scattering experiments.

ACKNOWLEDGMENTS

The authors thank Laura Fabbietti, Valentina Mantovani Sarti, Otón Vázquez Doce, Johann Haidenbauer, and other participants of the YITP workshop (YITP-T-18-07) for useful discussions. YK, TH and AO gratefully acknowledge the hospitality of the members in Technical University of Munich during their stay in Munich. This work is supported in part by the Grants-in-Aid for Scientific Research from JSPS (Nos. 19H05151, 19H05150, 19H01898, and 16K17694), by the Yukawa International Program for Quark-hadron Sciences (YIPQS), by the Polish National Science Center NCN under Maestro grant EC-2013/10/A/ST2/00106, by the National Natural Science Foundation of China (NSFC) and the Deutsche Forschungsgemeinschaft (DFG) through the funds provided to the Sino-German Collaborative Research Center “Symmetries and the Emergence of Structure in QCD” (NSFC Grant No. 11621131001, DFG Grant No. TRR110), by the NSFC under Grant No. 11847612 and No. 11835015, by the Chinese Academy of Sciences (CAS) under Grant No. QYZDB-SSW-SYS013 and No. XDPB09, and the CAS President’s International Fellowship Initiative (PIFI) under Grant No. 2020PM0020.

* yukikamiya@mail.itp.ac.cn

- [1] R. H. Dalitz and S. F. Tuan, Phys. Rev. Lett. **2**, 425 (1959); Annals Phys. **10**, 307 (1960); R. H. Dalitz, T. C. Wong, and G. Rajasekaran, Phys. Rev. **153**, 1617 (1967).
- [2] Y. Akaishi and T. Yamazaki, Phys. Rev. C **65**, 044005 (2002).
- [3] S. Ajimura *et al.* (J-PAC E15), Phys. Lett. B **789**, 620 (2019).
- [4] M. Bazzi *et al.* (SIDDHARTA), Phys. Lett. B **704**, 113 (2011); Nucl. Phys. A881, 88 (2012).
- [5] T. Hyodo and D. Jido, Prog. Part. Nucl. Phys. **67**, 55 (2012).
- [6] S. E. Koonin, Phys. Lett. **70B**, 43 (1977).
- [7] S. Cho *et al.* (ExHIC), Prog. Part. Nucl. Phys. **95**, 279 (2017).
- [8] J. Adams *et al.* (STAR), Phys. Rev. C **74**, 064906 (2006).
- [9] S. Acharya *et al.* (ALICE), Phys. Rev. C **99**, 024001 (2019).
- [10] L. Adamczyk *et al.* (STAR), Phys. Rev. Lett. **114**, 022301 (2015).
- [11] S. Acharya *et al.* (ALICE), Phys. Rev. Lett. **123**, 112002 (2019).
- [12] J. Adam *et al.* (STAR), Phys. Lett. B **790**, 490 (2019).
- [13] S. Acharya *et al.* (ALICE), arXiv:1905.13470 [nucl-ex].
- [14] S. Acharya *et al.* (ALICE), arXiv:1910.14407 [nucl-ex].
- [15] K. Morita, T. Furumoto, and A. Ohnishi, Phys. Rev. C **91**, 024916 (2015).
- [16] A. Ohnishi, K. Morita, K. Miyahara, and T. Hyodo, Nucl. Phys. A **954**, 294 (2016).
- [17] T. Hatsuda, K. Morita, A. Ohnishi, and K. Sasaki, Nucl. Phys. A **967**, 856 (2017).
- [18] J. Haidenbauer, Nucl. Phys. A **981**, 1 (2019).
- [19] K. Morita, S. Gongyo, T. Hatsuda, T. Hyodo, Y. Kamiya, and A. Ohnishi, arXiv:1908.05414 [nucl-th].
- [20] R. Lednicky, V. V. Lyuboshits, and V. L. Lyuboshits, Phys. Atomic Nuclei **61**, 2950 (1998).
- [21] K. Miyahara, T. Hyodo, and W. Weise, Phys. Rev. C **98**, 025201 (2018).
- [22] Y. Ikeda, T. Hyodo, and W. Weise, Phys. Lett. B **706**, 63 (2011); Nucl. Phys. A **881**, 98 (2012).
- [23] R. Lednicky and V. L. Lyuboshits, Sov. J. Nucl. Phys. **35**, 770 (1982) [Yad. Fiz. **35**, 1316 (1981)].
- [24] K. Morita, A. Ohnishi, F. Etminan, and T. Hatsuda, Phys. Rev. C **94**, 031901 (2016).
- [25] K. Miyahara and T. Hyodo, Phys. Rev. C **93**, 015201 (2016).
- [26] M. Tanabashi *et al.* (Particle Data Group), Phys. Rev. D **98**, 030001 (2018).